



Corrective osteotomies using patient-specific 3D-printed guides: a critical appraisal

Wouter Rosseels¹ · Michiel Herteleer^{2,3} · An Sermon^{2,4} · Stefaan Nijs^{2,4} · Harm Hoekstra^{2,4}

Received: 30 September 2017 / Accepted: 8 January 2018 / Published online: 12 January 2018
© Springer-Verlag GmbH Germany, part of Springer Nature 2018

Abstract

Introduction Over the last decade, the technique of 3D planning has found its way into trauma surgery. The use of this technique in corrective osteotomies for treatment of malunions provides the trauma surgeon with a powerful tool. However, this technique is not entirely straightforward. We aimed to define potential pitfalls of this technique and possible solutions to overcome these shortcomings.

Materials and methods Ten patients with either a uni-, bi- or triplanar malunion of the long bones were included in this study. These patients were divided into three groups: a weight-bearing group and a non-weight-bearing group, the latter was divided into the humerus group and the forearm group, subsequently. 2D correction parameters were defined and compared within every group, as well as the interpretations of 3D visualization.

Results The weight-bearing group revealed an undercorrection for almost all clinical measurements of the femur and tibia, while there was adequate matching of the osteotomies and of screw entry points in all cases. In the humerus group, coronal correction angles were nearly perfect in all cases, while axial and sagittal correction rates, however, differed substantially. Screw entry points and osteotomies were all at the level as planned. The forearm group showed undercorrection in multiple planes while there were good matching entry points for the screw trajectories.

Discussion Four major pitfalls were encountered using the 3D printing technique: (1) careful examination of the planned guide positioning is mandatory, since suboptimal intra-operative guide positioning is most likely the main cause of the incomplete correction; (2) the use of pre-drilled screw holes do not guarantee adequate screw positioning; (3) translation of bone fragments over the osteotomy planes in case of an oblique osteotomy is a potential hazard; (4) the depth of the osteotomy is hard to estimate, potentially leading to extensive cartilage damage.

Keywords Malunion · 3D-guided osteotomy · Osteosynthesis

Introduction

The surgical treatment of a malunion can be technically very demanding. However, 3D planning allows the surgeon to better visualize and understand the anatomy in full 3D

and digitally plan a corrective osteotomy to restore the normal anatomy and function. This planning is based on the patient's CT images, wherein multiple surgical approaches are taken into account. Hereby 3D planning has the potential to increase the accuracy of preoperative planning, increase the precision of surgical navigation, decrease postoperative complications, attain a more cost-effective use of operating rooms, as well as improvement of patient satisfaction [1, 2]. To that end, patient-specific surgical guides are designed to control the cutting and reduction according to the surgical plan, hereby aiming to improve the predictability of osteotomy procedures [1, 3–5].

Recently, we published a technical note on 3D-guided osteotomies for malunion of both articular and nonarticular limb fractures [6]. Osteotomies using 3D-printed patient-specific guides were very precise and this approach looks

✉ Harm Hoekstra
harm.hoekstra@uzleuven.be

¹ Faculty of Medicine, KU Leuven-University of Leuven, 3000 Leuven, Belgium

² Department of Trauma Surgery, University Hospitals Leuven, Herestraat 49, 3000 Leuven, Belgium

³ Department of Organ Systems, KU Leuven-University of Leuven, 3000 Leuven, Belgium

⁴ Department of Development and Regeneration, KU Leuven-University of Leuven, 3000 Leuven, Belgium

promising. Nevertheless, this technique is not entirely straightforward. The indications for this technique are often complex and challenging, wherein the surgical skills remain indispensable.

Here we describe in detail a case series, which include the planned and achieved results for 3D-guided osteotomies of the upper and lower limbs. By comparing these planned and achieved results, we aim to highlight the pitfalls of the technique and provide strategies to overcome difficulties.

Patients and methods

Patients

Ten patients with either a uni-, bi- or triplanar malunion of the long bones were included in this study. All patients got corrective osteotomies according to the 3D-printed patient-specific guides technique [6]. All surgical procedures were performed at the Department of Trauma Surgery of the University Hospitals Leuven between August 2014 and May 2016. Grouping was largely based on two criteria: weight-bearing (lower limb) versus non-weight-bearing (upper

Table 1 Definitions of 2D measurements listed per group

Humerus group	
Coordinate system	Axial plane perpendicular on mechanical axis. Mechanical axis from midpoint epicondyles to midpoint sphere humeral head. Coronal through epicondyles, perpendicular on axial
CCDA	Centrum-column-diaphyseal angle, angle measured in the coronal plane, defined in between projections of mechanical axis and line perpendicular to the coronal inflection points
Axial humeral torsion	Angle measured in the axial plane, defined in between projections of the distal transepicondylar line and the orientation of the humeral head defined by the axial inflection points
Varus/valgus	Angle measured in the coronal plane, defined in between projections of the mechanical axis and the joint line
Sagittal angle	Angle measured in the sagittal plane, defined in between projections of the mechanical axis and the sagittal anatomical neck line Ref. Poeze et al. Conservative management of proximal humeral fractures: can poor functional outcome be related to standard transscapular radiographic evaluation?
Forearm group	
Coordinate system	Based on radius. Axial plane perpendicular on mechanical axis. Mechanical axis as central line of a fitted cylinder of the 1/4th of the shaft region [7]
Radial inclination/tilt	Angle measured in the coronal plane, defined in between projections of a tangent line of the radial styloid and the concave sigmoid notch point and a line perpendicular to the mechanical axis
Ulnar length	Distance measured in the coronal plane in between projections of a tangent line to the sigmoid notch point and a tangent line to the ulnar head plateau
Volar tilt	Angle measured in the sagittal plane in between projections of a tangent line to the volar and dorsal rim and a line perpendicular to the mechanical axis
Radial and ulnar axial difference	Relative angles measured in the axial plane as projections of similar defined lines. For the radius this is a line defined from the radial styloid to the sigmoid notch. For the ulna, this is a line from the ulnar styloid to the opposite side of the ulnar head
Midshaft coronal angle	Angle measured in the coronal plane, in between projections of two lines defined by the center line of a fitted cylinder at the two fragments
Midshaft sagittal angle	Angle measured in the sagittal plane, in between projections of two lines defined by the center line of a fitted cylinder at the two fragments
Lower extremities group	
Coordinate system	Based on mechanical axis
mLDFA	Mechanical lateral distal femoral angle, angle measured in the coronal plane, in between projections of the femoral joint line and the mechanical axis
mMPTA	Mechanical medial proximal tibial angle, angle measured in the coronal plane, in between projections of the tibial joint line and the mechanical axis
Sagittal slope	Angle measured in the sagittal plane, in between projections of the tangent line at the plateau and the mechanical axis
mADTA	Mechanical anterior distal tibial angle, measured in between projections of a tangent line at the anterior and posterior rim of the distal tibia and the mechanical axis
mLDTA	Mechanical lateral distal tibial angle, angle measured in between projections of a tangent line at the tibial distal joint and the mechanical axis

limb) characteristics of the affected limbs; and second, the non-weight-bearing group was subdivided into the humerus group, which consists of only one long bone, and the forearm group, consisting of two closely connected bones, the radius and ulna. This study was completed in compliance with national legislation and the guidelines of the ethics committee of the University Hospitals Leuven.

Study design

The preoperative CT scan was segmented into 3D digital objects using Materialise Mimics (Materialise N.V., Leuven, Belgium). The 3D planning was defined in two steps. First, the necessary correction was determined based on the additional three-dimensional information from the patient's healthy contralateral side, which was used as a template for correction. By mirroring this template and overlaying it with the surgical side, the required correction was visualized and planned. Next, the osteosynthesis implants were positioned.

The planned corrections were translated in 2D through projection of landmarks and axes into the coronal, sagittal and axial planes using 3-Matic (Materialise N.V., Leuven, Belgium) as described in Table 1.

To transfer the virtual preoperative planning to the clinical reality, patient-specific guides were designed and produced in polyamide by selective laser sintering (SLS). The guides matched the specific anatomy of the patient and served as an intra-operative guidance for drilling screw holes and performing osteotomies according to the virtual preoperative planning.

After surgery, a postoperative quantification of the achieved correction was performed with the use of

postoperative CT scans similar to the quantification of the desired correction during the virtual preoperative planning.

Measurements

2D radiographic measurements and related landmarks to define the planned and achieved correction per group are listed in Table 1. The planned correction angle Δ for each of these parameters was defined as: $\Delta = \text{planned angle} - \text{preoperative angle}$. A negative Δ implies the need to reduce the measured parameter. A positive Δ implies the need to enlarge the measured parameter. After surgery with patient-specific guides, a postoperative CT scan was made and converted into 3D digital objects and registered into the same anatomical reference coordinate system as used for the preoperative planning. By projecting the anatomical landmarks and the axes, the achieved correction angle δ was obtained: $\delta = \text{outcome angle} - \text{preoperative angle}$. By comparing the planned and achieved correction angle the success rate of the guided surgery can be determined, in which the absolute difference $|\Delta - \delta|$ shows the difference in degrees between planned and achieved correction. Subsequently, the success rate σ was defined as: $\sigma = 1 - ((\Delta - \delta)/\Delta)$. A success rate of more than 100% implies an overcorrection. A negative success rate implies an achieved correction in the opposite than desired angle. A 100% success rate implies the performed correction was performed exactly as planned.

Conventional 2D clinical measurements alone do not provide enough insight for making suggestions on improvement of the procedure. Therefore, the 2D measurements were complemented with interpretations from the 3D visualization, including the final position of the plate and screws

Table 2 Planned and achieved correction angles, and success rates of lower extremity-guided osteotomy

Lower extremities group	2D measurement	Δ , planned correction angle (°)	δ , achieved corrected angle (°)	Absolute difference planned vs achieved (°) $\Delta - \delta$	Percentage of the correction achieved $\sigma = 1 - ((\Delta - \delta)/\Delta)$ (%)
Distal femur case A	Coronal mL DFA	5.2	1.7	3.5	32.5
	Axial	0.6	0.4	0.2	63.5
	Sagittal	1.8	2.0	-0.2	111.1
Distal tibia case B	Coronal mL DTA	9.3	9.0	0.3	96.8
	Axial	11.2	21.8	-10.6	195.1
	Sagittal mADTA	6.3	6.2	0.0	99.5
Tibia plateau case C	Coronal mMP TA	-12.3	-1.5	-10.8	12.0
	Sagittal slope	15.5	4.6	10.9	29.9
Midshaft femur case D	Coronal mL DFA	-11.1	-10.8	-0.4	96.8
	Axial	-1.8	2.1	-3.9	-114.4
	Sagittal	-0.6	1.5	-2.1	-272.7

mL DFA mechanical lateral distal femoral angle, *mL DTA* mechanical lateral distal tibial angle, *mADTA* mechanical anterior distal tibial angle, *mMP TA* mechanical medial proximal tibial angle

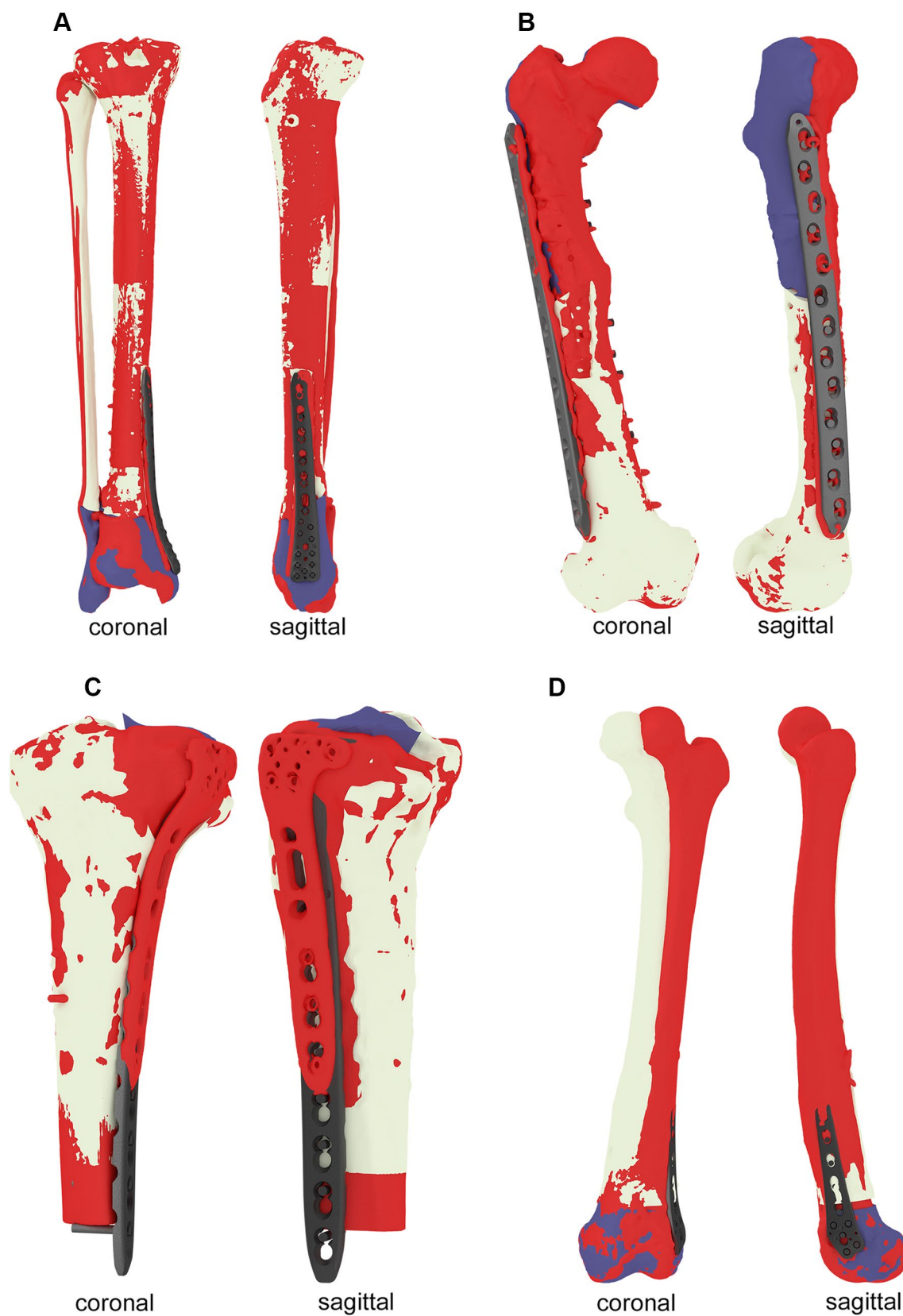


Fig. 1 Three-dimensional visualization of lower extremity correction osteotomy. Bone color: original preoperative scanned position. Purple color: reduced fragment. Gray color: planned plate position. Red

color: postoperative fragment and plate position. Case A, coronal and sagittal view; case B, coronal and sagittal view; case C, coronal and sagittal view; case D, coronal and sagittal view

compared to the planned position and an overall impression of the achieved reduction of the fragments.

Results

Weight-bearing: lower extremities group

The results of the weight-bearing group are shown in Table 2 and Fig. 1. The results of the weight-bearing group were hard to interpret, given the inherent differences between the performed procedures. From a 3D reconstructive point of view, only two out of four cases could be reported as satisfying: the best correction was achieved for the coronal correction of the distal tibia and the coronal correction of the mid-shaft femur. The vast majority of the corrections, however, revealed undercorrection. Three-dimensional visual control demonstrated adequate matching of the osteotomies and of the screw entry points in all cases.

Non-weight-bearing single bone: humerus group

The results of the non-weight-bearing single-bone group are shown in Table 3 and Fig. 2. In all cases, coronal correction angles were nearly perfect. The best results were obtained in the proximal humerus malunion group. Axial and sagittal correction rates, however, differed substantially. The three-dimensional visualization showed screw entry points and osteotomies at the preplanned level. On the contrary, the screw trajectories deviated in most cases. The position of the plate in the proximal humerus osteotomy group tended to be slightly more anterior than planned. Regarding the height, the plates were fitted somewhat in a more proximal position.

Non-weight-bearing dual bone: forearm group

The results of the non-weight-bearing correlated bone group are depicted in Table 4 and Fig. 3. The combined distal radius and ulna osteotomy were undercorrected in multiple planes. Both patients in the forearm group showed high correction angles in the axial plane of the ulna. In contrast, in both cases some of the planned and achieved corrections were small, leading to disproportional high correction rates. The three-dimensional visualization shows good matching entry points for the screw trajectories; however, the direction of the screw trajectories differed as planned for, even for the used non-variable angle locking plate and screws. Good guide and plate positioning was achieved in half of the bones. One radius guide was positioned too proximal, while one ulnar guide was positioned more dorsal than planned. In case A, the ulnar plate showed substantial deformation.

Discussion

The primary aim of this study was to investigate the accuracy of preoperative planned osteotomies, using 3D-printed patient-specific guides, highlight the causes of the imperfections and provide solutions. Therefore, we reviewed ten cases of patients with a long bone malunion who required a corrective osteotomy for functional or esthetic reasons. Both angular measurements and visual information were used in an attempt to provide strategies to improve the outcome.

The long bone osteotomy cases were grouped as either weight-bearing—lower extremities—or

Table 3 Planned and achieved correction angles, and success rates of humerus-guided osteotomy

Humerus group	2D measurement	Δ , planned correction angle (°)	δ , achieved corrected angle (°)	Absolute difference planned vs achieved (°) $\Delta - \delta$	Percentage of the correction achieved $\sigma = 1 - ((\Delta - \delta)/\Delta)$ (%)
Proximal humerus case A	Coronal CCDA	11.5	11.3	0.2	98.3
	Axial humeral torsion	-6.0	-8.4	2.4	140.4
	Sagittal angle	5.1	5.4	0.3	105.3
Proximal humerus case B	Coronal CCDA	25.0	25.3	0.3	101.0
	Axial humeral torsion	-5.5	1.0	6.4	-17.4
	Sagittal angle	0.8	-4.0	4.9	-472.9
Proximal humerus case C	Coronal CCDA	22.6	21.4	1.2	94.6
	Axial humeral torsion	11.1	13.6	2.6	123.3
	Sagittal angle	-16.2	-11.5	4.6	71.3
Distal humerus case D	Coronal varus/valgus	-24.8	-22.2	2.6	89.5
	Axial humeral torsion	21.5	17.5	4.1	81.1
	Sagittal angle	0.6	6.1	5.5	1051

CCDA centrum-column-diaphyseal angle

Fig. 2 Three-dimensional visualization of humerus correction osteotomy. Bone color: original preoperative scanned position. Purple color: reduced fragment. Gray color: planned plate position. Red color: postoperative fragment and plate position. Case A, coronal and sagittal view; case B, coronal and sagittal view; case C, coronal and sagittal view; case D, coronal and sagittal view

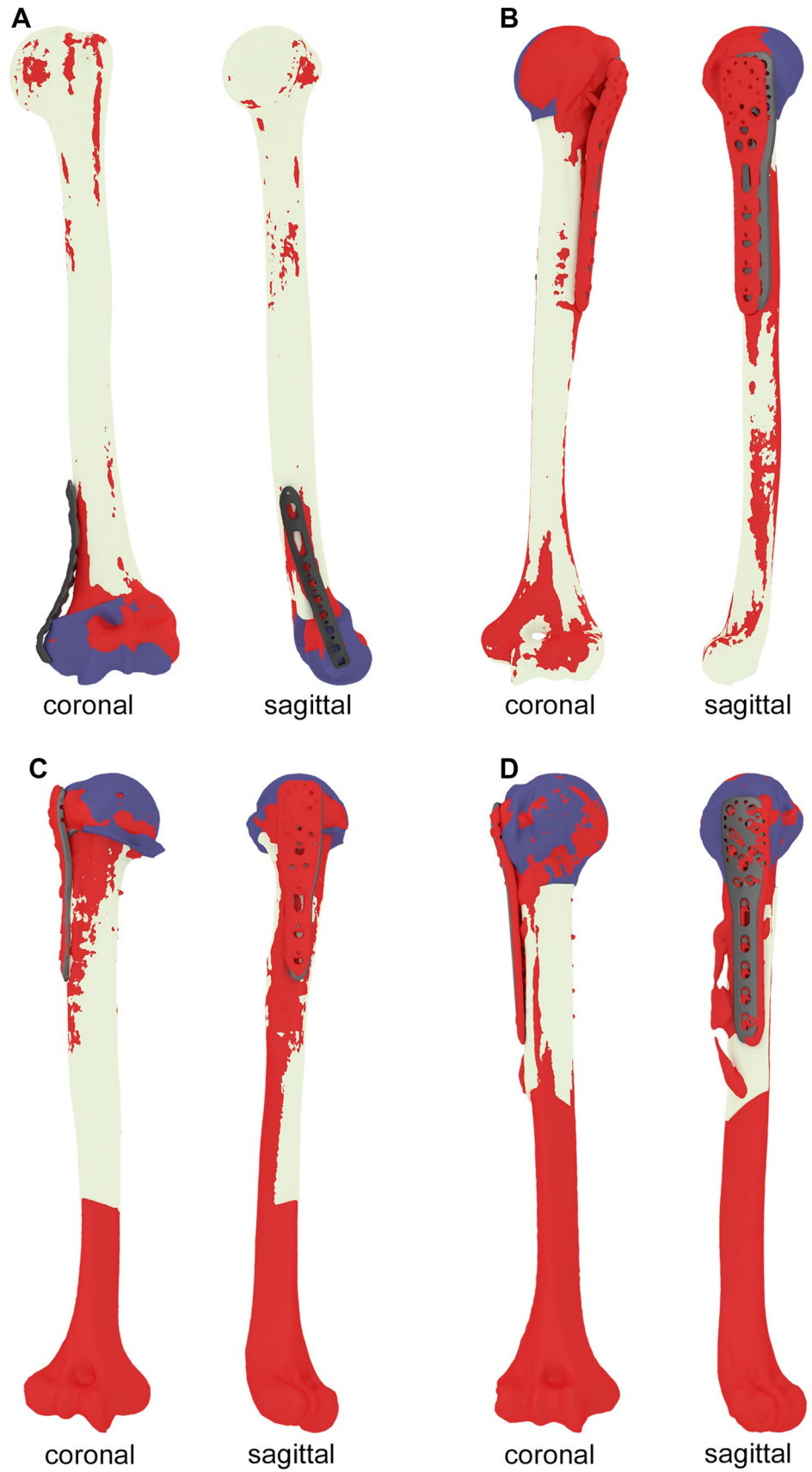


Table 4 Planned and achieved correction angles, and success rates of forearm-guided osteotomy

Forearm group	2D measurement	Δ , planned correction angle (°)	δ , achieved corrected angle (°)	Absolute difference planned vs achieved (°) $\Delta - \delta$	Percentage of the correction achieved $\sigma = 1 - ((\Delta - \delta)/\Delta)$ (%)
Distal radius–ulna case A	Coronal radius	-4.6	-2.0	-2.6	43.0
	Sagittal radius	22.2	14.8	7.4	66.7
	Axial difference radius	-6.0	-2.6	-3.4	43.6
	Ulnar length	0.3	-0.2	0.4	-57.1
	Axial difference ulna	-42.0	-32.0	-10.0	76.3
Midshaft radius case B	Coronal radius	-1.6	-1.3	-0.3	83.0
	Sagittal radius	-17.1	-14.5	-2.6	84.8
	Axial difference radius	-5.9	-7.8	1.9	131.8
	Coronal ulna	0.9	-1.5	2.3	-165.9
	Sagittal ulna	-12.2	-6.5	-5.7	53.1
	Axial difference ulna	-29.4	-21.2	-8.2	72.2

non-weight-bearing—humerus and forearm. Regarding the lower extremities, almost all clinical measurements of the femur and tibia revealed an undercorrection postoperatively. Particularly, the tibia plateau osteotomy lagged well behind what was planned, in both the coronal and sagittal plane. Next, the three-dimensional visualization of the planned and achieved osteotomy of the distal femur showed that the planned cortical bone resection prior to plate fixation was not performed sufficiently resulting in coronal undercorrection. Furthermore, translation in the closing wedge osteotomy of the distal tibia and distal femur did not significantly affect the clinical 2D measurements. Three-dimensional visual control showed adequate matching of the osteotomies and of screw entry points in all cases.

The main indications for correction in the humerus group were varus or valgus deformities. In all cases, the coronal correction angle was more pronounced than the axial correction angle. The 2D clinical measurements showed similar, nearly perfect coronal correction rates for all proximal humerus malunion cases. The correction rates in the axial and sagittal planes, however, differed substantially between our patients. Like in the weight-bearing group, osteotomies and screw entry points matched in all cases. However, the screw trajectories deviated from the planned position. The guide and thus the plate fitted slightly more anterior and proximal than expected.

The forearm group consisted of a combined distal radius and ulna osteotomy as well as a radius shaft osteotomy. Despite the fact that the combined distal radius and ulna osteotomy was technically highly demanding, the postoperative measurements showed only a slight sagittal undercorrection. Both patients in the forearm group showed high correction angles in the axial plane of the ulna. In parallel with the weight-bearing and humerus groups, most of the planned and achieved corrections turned out to be relatively

small, what led to excessive correction rates for some measurements. Three-dimensional visual control showed similar results for the weight-bearing and humerus groups. Our results showed limited deviations of the screw trajectories but a good matching of the screw entry points.

To find the root cause for the deviation of the screw trajectories in the weight-bearing group, we should focus on the ease of access and the straightforwardness of the planned procedure. The load-bearing characteristics might have altered the results after a period of load bearing, in which the fragments can move due to the applied forces. Furthermore, difficulties were encountered while using this technique for a corrective articular osteotomy of the tibia plateau. In these cases, preference was given to cut just into the subchondral bone, leaving the cartilage partially intact. With the patient-specific guides, however, the depth of the osteotomy is hard to estimate, potentially leading to extensive cartilage damage. Even when the guide is designed in such a way that the depth of the osteotomy is restrained in multiple directions, the reduction of a corrective articular osteotomy remains very difficult.

In the non-weight-bearing humerus group, the use of pre-drilled screw holes does not guarantee that the screws are inserted into the plate as planned for, due to the variable angle characteristics of the plates and screws. This might be the most important factor leading to an inadequate axial correction. To overcome deviating screw trajectories the surgeon should consider to use non-variable angle locking plates and screws to better control the direction of insertion of the screws during the operation. Pre-drilled screw holes do not guarantee that the screws are applied in such relation to the plate as planned for, due to the 30° conus of the used variable angle locking compression plates (DePuy Synthes). Subsequently, the accuracy of the overall bone reduction may be decreased.



Fig. 3 Three-dimensional visualization of forearm correction osteotomy. Bone color: original preoperative scanned position. Purple color: reduced fragment. Gray color: planned plate position. Red

color: postoperative fragment and plate position. Case A, coronal and sagittal view; case B, forearm coronal and sagittal view, radius coronal and sagittal view, and ulna coronal and $\frac{3}{4}$ view

Nevertheless, non-variable angle locking screws were also found to imply deviating screw trajectories on the forearm to some extent. The use of hand screwdrivers instead of a power tool might minimize this phenomenon.

Another possible pitfall is translation of bone fragments over the osteotomy planes in case of an oblique osteotomy due to the applied compression. To avoid translation of bone fragments in case of an oblique osteotomy, Kataoka et al. [8] suggest to use custom-made plates that have optimal contact with the bone surface. In addition, an incorporated

mechanical block or visual reference through a stepped cut osteotomy can prevent translation errors.

The same pitfall, with deviating screw trajectories, was also observed in the forearm group. The three-dimensional visualization of the forearm group also showed less accurate plate application on both the distal radius and ulna. The radius and ulna are interrelated, act as a joint and should be considered as a whole for the planning a corrective osteotomy. Correct guide positioning of both bones is difficult to achieve due to the pronounced cylindrical shape. Therefore, careful examination of the planned guide positioning is

mandatory since suboptimal intra-operative guide positioning, together with hardware deviations, is most likely the main cause of the incomplete correction. A similar conclusion, concerning the importance of optimal guide positioning, was drawn by Honingmann et al. [9] who stressed the importance of optimal guide positioning in a case report about a corrective palmar opening wedge osteotomy of the distal radius. The exact positioning of the guide is accomplished by sufficient exposure of the guide to the circumference of the bone.

Although this study is to our knowledge the first study that reports on desired and achieved corrections using specific osteotomy guides, highlighting the pitfalls and providing solutions, there are some limitations. First, the results were not linked to the clinical outcome. The main objective of this study was to critically evaluate the process of the 3D-printed patient-specific guide technique from a to z independent of the clinical outcome. Therefore, both planned and achieved correction rates were chosen to be defined independent of the clinical outcome. A second limitation is the use of percentages to express the success of the performed correction, since percentages give us an idea of the relative but not the absolute degree of correction. Third, the number of patients was relatively small and the group of patients was heterogeneous.

The 3D-printed patient-specific guide technique makes the preoperative planning more straightforward to execute, without the need for excessive bone cortex removal or multiple fragments, and it increases the chances of success. However, the indications for the 3D-printed patient-specific guide technique are rather complex and despite the optimism, this technique also has its limitations. Optimal guide positioning is the first important step during this procedure, since inadequate guide positioning, suboptimal pre-drilled holes (or K-wires) and subsequently suboptimal osteotomy lead to inaccurate corrections in multiple planes. The main limiting step of this technique, however, remains the reduction. Performing the reduction with the current implants may lead to errors. This could be minimized by applying custom-made plates, using locking metal sleeves or other devices so that the screws can be applied in such relation to the plate as planned for, and using manual drivers instead of a power tool. Another way to optimize the reduction would be to perform a more constrained reduction, for example, by performing a stepped cut osteotomy. Next, when planning small corrections, one should be aware that these small corrections result in less predictable outcomes. Finally, taking into

account that undercorrection was more frequently observed than overcorrection, one should anticipate this while performing the osteotomy.

Acknowledgements Els Bruynooghe; Marterialise, Leuven, Belgium.

Compliance with ethical standards

Conflict of interest Wouter Rosseels, Michiel Herteleer, An Sermon, Stefaan Nijs and Harm Hoekstra have no conflicts of interest.

Ethical approval The study protocol was approved by the Ethics Committee of the University Hospitals Leuven. The study was conducted in accordance with the principles of the Declaration of Helsinki.

Informed consent A written informed consent was obtained from all patients or legal guardians.

References

1. Victor J, Premanathan A. Virtual 3D planning and patient specific surgical guides for osteotomies around the knee: a feasibility and proof-of-concept study. *Bone Jt J*. 2013;95:153–8.
2. Rengier F, Mehndiratte A, von Tengg-Kobligh H, Zechmann CM, Unterhinninghofen R, Kauczor HU, Giesel FL. 3D printing based on imaging data: review of medical applications. *Int J CARS*. 2010;5:335–41.
3. Kunz M, Ma B, Rudan JF, Ellis RE, Pichora DR. Image-guided distal radius osteotomy using patient-specific instrument guides. *J Hand Surg Am*. 2013;38:1618–24.
4. Schweizer A, Frnstahl P, Nagy L. Three-dimensional correction of distal radius intra-articular malunions using patient-specific drill guides. *J Hand Surg Am*. 2013;38:2339–47.
5. Takeyasu Y, Oka K, Miyake J, Kataoka T, Moritomo H, Murase T. Preoperative computer simulation-based three-dimensional corrective osteotomy for cubitus varus deformity with use of a custom-designed surgical device. *J Bone Jt Surg Am*. 2013;95:1731–9.
6. Hoekstra H, Rosseels W, Sermon A, Nijs S. Corrective limb osteotomy using patient specific 3D-printed guides: A technical note. *Injury*. 2016;47(10):2375–80.
7. Grood ES, Suntay WJ. A joint coordinate system for the clinical description of three-dimensional motions: application to the knee. *J Biomech Eng*. 1983;105(2):136–44.
8. Kataoka T, Oka K, Miyake J, Omori S, Tanaka H, Murase T. 3-Dimensional prebent plate fixation in corrective osteotomy of malunited upper extremity fractures using a real-sized plastic bone model prepared by preoperative computer simulation. *J Hand Surg*. 2013;38A:909–19.
9. Honingmann P, Thieringer F, Steiger R, Haefeli M, Schumacher R, Henning J. A simple 3-dimensional printed aid for a corrective palmar opening wedge os teotomy of the distal radius. *J Hand Surg Am*. 2016;41:464–9.